Global NEST Journal, Vol 25, No X, pp 1-9

Air pollution monitoring approach using atomic orbital search algorithm with deep learning driven

Saravanan R.[1]*, Godwin Ponsam J.[2], Sathiya V.[3] and Saranya G.[4]
[1]Department of Computer Science and Engineering, Rajalakshmi Institute of Technology, Chennai 600124, Tamil Nadu, India
[2] Department of Networking and Communications, SRM Institute of Science and Technology, Kattankulathur, 603202, Tamil Nadu, India
[3]Department of Computer Science and Engineering, Panimalar Engineering College, Chennai, 600123, Tamil Nadu, India
[4]Department of Computer Science and Engineering, Amrita School of Computing, Amrita Vishwa Vidyapeetham, Chennai, Tamil Nadu, India
Received: 08/09/2023, Accepted: 05/11/2023, Available online: 10/11/2023
*to whom all correspondence should be addressed: e-mail: dr.saravananrcse@gmail.com
https://doi.org/10.30955/gnj.005373

Graphical abstract

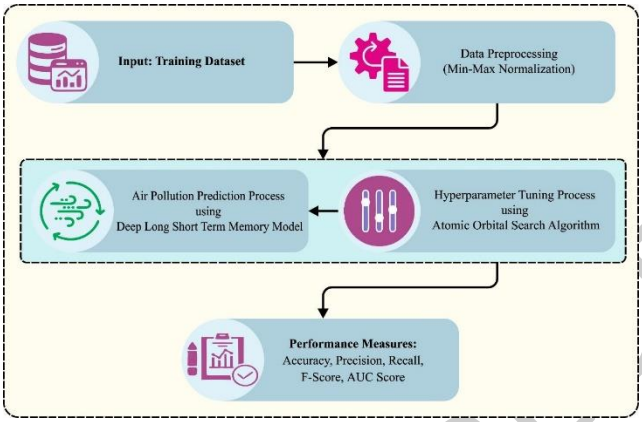

Abstract

Air pollution is a major reason for health-related issues and weather changes, one of humanity's most dangerous problems. It is the most crucial environmental issue in the 21st century and has attracted global attention. These challenges are exacerbated by an overabundance of automobiles, industrial output, pollution, transportation, fuel consumption, and energy generation. Therefore, air pollution prediction was developed vital. Air pollution monitoring is the procedure of analyzing and measuring the air quality in a certain place to develop the levels of several pollutants and contaminants present. Monitoring air pollution is vital to understand its sources and effects on the environment and human health, and for executing methods for mitigating its effects. Deep learning (DL) approaches are employed for air pollution predicting methods. Therefore, this study develops an Atomic Orbital Search Algorithm with a Deep Learning-Driven Air Pollution Monitoring (AOSADL-APM) approach. The purpose of the AOSADL-APM technique is to predict and classify the presence of air pollutants. In the presented AOSADL-APM technique, the min-max normalization approach is applied for data preprocessing. For air pollution prediction and classification, the AOSADL-APM technique applies the deep long short-term memory (DLSTM) methodology. To enhance the performance of the AOSADL-APM technique, the AOSA-based hyperparameter tuning has been developed. The simulation results of the AOSADL-APM technique were tested using the benchmark dataset. The widespread outcome analyzed the greater solution of the AOSADL-APM algorithm compared to existing approaches.

Keywords: Air pollution, deep learning, data-driven approach, hyperparameter tuning, prediction

1. Introduction

Energy consumption and its effects are unavoidable in current world human actions. The man-made causes of air pollution comprise releases from industrial plants; automobiles; kerosene; aerosol cans, and planes; coal burning of straw, among others. Elshaboury, N., *et al.* (2023) described different hazardous pollutants such as NO2, CO2, COss, O3, NH3, SO2, Pb, Particulate Matter (PM), etc. have been released into our surroundings regularly. Drewil, G.I. *et al.* (2022) discussed about air pollution may lead plenty of severe diseases in human beings, from pneumonia to lung cancer, bronchitis to heart disease, and so on. Huang, L., *et al.* (2021) explained insufficient air conditions cause other existing environmental problems such as acid rain, early death, decreased visibility, smog, aerosol formation, weather changes, and global warming. Researchers recognized that air pollution carries the ability to harmfully involve previous monuments. Environmental emissions of industries and power stations, agricultural disposal, vehicle emissions, etc. can be accountable for increasing greenhouse gases. Abirami, S *et al.* (2023) implements the greenhouse gases negatively impact climatic factors and accordingly the growth of plants. Greenhouse gases and inorganic carbon emissions also impact plant-soil relations. Meteorological conditions not only affect animals and humans, but productivity and agricultural factors are also highly affected. Financial losses are also related to implications. Jamei, M., *et al.* (2022) expose the Air Quality Index (AQI), an evaluation factor, could be directly relevant to medical management. A high degree of AQI specifies a very harmful

experience for human habitation. Sonawani, S., *et al.* (2021) proved the needs of forecast the AQI in advance inspired the researchers to monitor as well as model the quality of air. Predicting and monitoring AQI, principally in urban regions is an essential and different activity for raising development of motor and industries. Majorly, air quality-related research and researchers aim emerging nations, although the focus on highly dangerous contaminants such as PM2.5 is established at multiple levels in developing countries.

Wang S., *et al.* (2023) executes the quantification, alleviation, and assessment of these impacts need techniques for evaluating the involvement of traffic volumes in air pollution. Conventionally, this is implemented by incorporating an evaluation (both noticed or modelled) of traffic volume, or instead of the allied pollution generation evaluated with weather monitoring in distribution techniques that determine a set of partial differential equations (PDE) for estimating the preferred pollution distributions. Gu, Y., *et al.* (2022) introduce the approach is limited in 3 processes, namely, the PDE method is computationally costly, needs significant field capability, and cumbersome to configure for more geographical positions. The computational cost limits the meshes that could be determined with respect to the spatial resolution, spatial level, and finally, the multiple discrete sources of pollution. Wardana, I.N.K., *et al.* (2021) explored the several techniques have been developed for forecasting pollutant concentrations because of the development of artificial intelligence (AI). These techniques are categorized into two types, namely non-deep learning (DL) and DL methods. Shu, Y *et al.* (2023) implements the non-DL approaches comprise two major techniques such as statistical and deterministic ones. Other algorithm leverages the ability of DL for establishing fast estimates, which is measured with some domain size.

This study develops an Atomic Orbital Search Algorithm with a Deep Learning-Driven Air Pollution Monitoring (AOSADL-APM) approach. The purpose of the AOSADL-APM technique is to predict and classify the presence of air pollutants. In the presented AOSADL-APM technique, the min-max normalization approach is applied for data preprocessing. For air pollution prediction and classification, the AOSADL-APM technique applies the deep long short-term memory (DLSTM) methodology. To enhance the performance of the AOSADL-APM technique, the AOSA-based hyperparameter tuning has been developed. The simulation results of the AOSADL-APM technique were tested utilizing the benchmark database.

2. Related works

Wu, C.L *et al.* (2023) developed a new DL-based hybrid methodology of Res-GCN-BiLSTM integrating the ResNets, Bi-LSTM, and GCN was developed. Primarily, cluster analysis and auto-correlation analysis are employed. Furthermore, the detected spatiotemporal attributes are adequately leveraged, and the monitoring network topological data, and meteorology and auxiliary pollutants are adaptably combined. Lin *et al.* (2021) implemented a Gated Recurrent Unit (GRU) DL network model for developing diverse prediction methods, which address several spatial and temporal conditions, followed by developing an ensemble learning predicting algorithm termed Multiple Linear Regression based GRu (MLE-GRU) depending on multilinear regression approach to incorporated DL prediction methods. Gilik, A *et al.* (2022) introduced a supervised technique for predicting air pollution with the help of actual sensor data and carrying pattern among cities. The incorporation of CNN and LSTM-DNN techniques has been developed. Two techniques were implemented: the uni-variate model comprises the data of a single pollutant but the multi-variate model includes the data of every pollutant and meteorological information for forecasting.

Dairi, A., *et al.* (2021) developed an adaptable and effective DL-driven algorithm for predicting the measurement of environmental pollutants. This study presents initially the standard VAE and attention methods to design the prediction model approach dependent on the innovative integrated multiple-directed attention (IMDA) DL technique. Du *et al.* (2019) present a new DL approach for the quality of air that learns the spatial-temporal correlation features and connection of multiple variate air quality compared to time-series data by the hybrid DL method. Because of the non-linear and dynamic features of multiple variate quality of air time-series data, the base components of the presented method contain 1D-CNNs and a Bi-LSTM approach. Heydari *et al.* (2022) designed a novel hybrid intelligent approach that depends on an LSTM and multiverse optimizer approach (MVO). In this introduced method, the LSTM approach has a predictor engine to forecast the quantity of generated SO2 and NO2 by the combination of Cycle Power Plant, but the MVO algorithm has been exploited for enhancing the LSTM parameters to attain minimum predictive methods.

Arsov, M *et al.* (2021) developed utilizing the RNN technique with LSTM modules for forecasting the level of PM10 particles. This method utilizes earlier quality of air evaluated data from sensors positioned at numerous places in Skopje and climatic circumstances, namely, humidity and temperature. Hardini *et al.* (2023) suggested an air quality estimation method to simplify forthcoming predictions. The research includes three primary processes, namely, measuring Air Quality, data production, and AQI prediction. The Data production method contains real-time data gathering and formatting to provide similarity with the following methods. In this study, the Sparse Spectrum GPR (SS-GPR) approach was utilized for predicting AQI, whereas the cloud technique could be implemented for measuring air quality.

3. The proposed model

In this manuscript, we have presented an automated air pollution monitoring approach named the AOSADL-APM approach. The purpose of the AOSADL-APM technique is to predict and classify the presence of air pollutants. In the presented AOSADL-APM technique, three subprocesses are involved, namely, data normalization, DLSTM-based

prediction, and AOSA-based hyperparameter tuning. Figure 1 displays the entire flow of the AOSADL-APM algorithm.

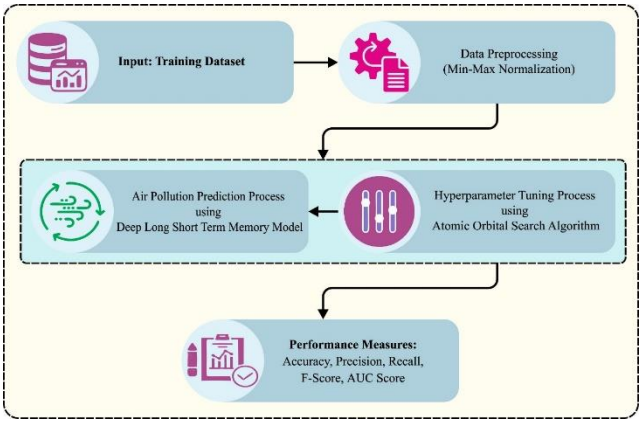

Figure 1. Overall flow of the AOSADL-APM approach

3.1. Data normalization

In the presented AOSADL-APM technique, the min-max normalization approach is applied for data preprocessing. Min-max normalized, also called feature scaling or min-max scaling, is a data preprocessed system utilized in ML and data analysis for rescaling numerical features to a certain range. The purpose of this method is to change the data thus it falls in the existing range, standardly between zeros and one, or any other preferred range like (-1, 1).

3.2. Prediction using the DLSTM model

For air pollution prediction and classification, the AOSADL-APM system applies the DLSTM model. To predict and understand sequences, Tang, W *et al.* (2023) researcher works have turned to the RNN design called deep LSTM. Different from classical RNN, which could experience the problem of gradient disappearing while training on long sequences, LSTM is enhanced for identifying long-term dependency. Figure 2 defines the structure of LSTM.

LSTM is built with a memory cell that can be able to retain data for a longer period, which allows the network to utilize and retain significant data from early time steps. In addition, LSTM has a gate that controls the information flow, involving forget, input, and output gates. Surendran R., *et al.* (2023) mention the gates can be accountable for regulating the outgoing and incoming data from the memory units, which enables the Lstm to choose to retain or discard data according to its significance.

Deep LSTM network pertains to the employ of different LSTM layers that are hierarchically ordered. The succeeding layer of the LSTM structure receives the output from the prior layers, which enables the NN to obtain a hierarchical visualization of the input data. An initial step includes the application of the forget gate, represented by $g(t)$ for initiating the LSTM model that plays a critical role in determining that data in the prior state must be discarded by the memory cells. The forget gate $g(t)$ can be given as follows:

$$f\,g(t)=\sigma(\alpha_{fg}x(t)+\beta_{fg}h(t-1)+\delta_{fg}) \quad (1)$$

Where $fg(t)$ shows the forget gate that considers the value ranges from zero to one. The logistic sigmoid function, 0 is employed. The configurable weighted matrix and the bias vector are represented by $\alpha_{fg},\beta_{fg},and\ \delta_{fg}$

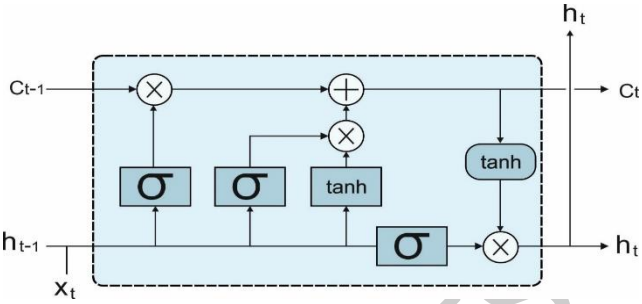

Figure 2. LSTM architecture

Consequently, the next step concentrates on defining the data that should be integrated as memory cells for upgrading purposes. The input gate (t) can be defined by the sigmoid function and is accountable for detecting the values that should be upgraded. Furthermore, a *tanh* hyperbolic tangent layer can be used for generating a potential upgrade vector, represented by (t). Eqs. (2) and (3) give a comprehensive description of computation for $i(t)$ and $C(t)$:

$$i(t)=\sigma(\beta_i h(t-1)+\alpha_i x(t)+\delta_i) \quad (2)$$

$$c(t)=\tanh(\beta_c h(t-1)+\alpha_c x(t)+\delta_c) \quad (3)$$

Consider the assumed values within [0,1]. The α_j, β_j, and δ_i symbols represent a series of trained parameters connected to the input gate, while $\alpha_c,\beta_c \text{ and } \delta_c$, pertain to a series of trained parameters.

When the purpose is made regarding the information that can be preserved and eliminated, the cell layer, represented by (t) that has been exposed to the updating method is evaluated by the following expression:

$$c(t)=i(t)\circ c(t)+fg(t)\circ c(t-1) \quad (4)$$

Where $\circ$ represents component-wise multiplicity. The term "$g(t)\circ c(t-1)$" shows the information that is collected $c(t-1)$, while the term "$\circ\, c(t)$" denotes the new data that is incorporated as the cell layer.

Finally, the step involves the calculation of the output gate that roles as a major part in defining the layer viz., hidden $h(t)$. The calculation of output, represented by (t) can be accomplished by using the sigmoid function. At the same time, the output has been accomplished by implementing the multi-operation among $o(t)$ and *tanh* hyperbolic tangent output. The process is demonstrated as:

$$o(t)=\sigma\left(\alpha_o x(t)+\beta_0 h(t-1)+\delta_o\right) \quad (5)$$

$$h(t)=o(t)\circ\tanh\left(c(t)\right) \quad (6)$$

Where $o(t)$ shows the vector [0, 1], $\alpha_o,\beta_o \text{ and } \delta_o$ denotes trained parameters related to the input gate.

3.3. Hyperparameter tuning using AOSA

To better the performance of the AOSADL-APM methodology, the AOSA-based hyperparameter tuning was established. According to the concept of atomic theory and quantum mechanics, the study presents an AOSA, mathematical expression that describes the wave-like behaviour of one or two electrons in an atom. The underlying concept behind the AOS approach is to use quantum-based atomic theory to address problems such as electron density configuration and atoms' ability to emit or absorb energy. The AOS techniques explore multiple solution possibilities (*X*) in the quantum-based atomic model that represents the electron encircling the nucleus. In this method, the thin, concentric spherical layers of the electron cloud near the nucleus have been designated as a searching space. In the search space, all electrons are shown by the solution candidate (X_i), with some decision variable (X_{ij}) defining the location of the solution candidate. The mathematical equation is given below:

$$X=\begin{bmatrix} X_1 \\ X_2 \\ \vdots \\ X_i \\ \vdots \\ X_m \end{bmatrix}=\begin{bmatrix} x_1^1 & x_1^2 & \ldots & x_1^j & \ldots & x_1^d \\ x_2^1 & x_2^2 & \ldots & x_2^j & \ldots & x_2^d \\ \vdots & \vdots & \ldots & \vdots & \ldots & \vdots \\ x_i^1 & x_i^2 & \ldots & x_i^j & \ldots & x_i^d \\ \vdots & \vdots & \ldots & \vdots & \ldots & \vdots \\ x_m^1 & x_m^2 & \ldots & x_m^j & \ldots & x_m^d \end{bmatrix}, i=1,2,\ldots,m., j=1,2,\ldots,d. \quad (7)$$

In Eq. (7), *m* signifies the solution candidates (number of electrons) inside the electron cloud (search space), and *d* indicates the dimensionality of the problem defining the electrons (candidate position). The starting position of the electron within the electron cloud is specified randomly according to the mathematical formula as follows:

$$x_i^j(0)=x_{i,\min}^j+rand.\left(x_{i,\max}^j-x_j\right), \begin{cases} i=1,2,\ldots,m. \\ j=1,2,\ldots,d. \end{cases} \quad (8)$$

In Eq. (8), $x_i^j(0)$ indicates the initial position of the solution candidate; $x_{i,max}^j$ and $x_{i,\min}^j$ shows the indication of the maximum and minimum boundaries of the jthdecision variables, correspondingly; *rand* indicates a random distribution value [0,1].

With a lower energy level, the electron corresponds to the solution candidate with the great objective function value. In the mathematical modelling, those with lower objective function value show electrons with the highest level of energy. The value of an objective function of different candidate solutions is kept in the subsequent formula

$$E=\begin{bmatrix} E_1 \\ E_2 \\ \vdots \\ E_i \\ \vdots \\ E_m \end{bmatrix}, i=1,2,\ldots,m. \quad (9)$$

In Eq. (9), *E* indicates the vector considering the values of the main function, E_i specifies the energy level of the i^{th} solution candidate and *m* signifies the amount of solution candidates within the searching range. The entire imaginary layer has some solution candidates based on the specified specifics of defining the electron position using PDF. Hence, the mathematical equation represents the vector of the placement of the solution candidate (X^k) and the value of the main function (E^K) in the imaginary layer:

$$E^k=\begin{bmatrix} E_1^k \\ E_2^k \\ \vdots \\ E_i^k \\ \vdots \\ E_p^n \end{bmatrix}, \begin{cases} i=1,2,\ldots,p. \\ k=1,2,\ldots,n. \end{cases} \quad (10)$$

In Eq. (10), E_j^k shows the k^{th} imaginary layer of the i^{th} solution candidate's objective function value, the integer *n* specifies the maximum number of imagined levels, X_i^k displays the k^{th} imaginary layer's i^{th} candidate solution, *p* shows the imaginary layer of k^{th} solution candidate and *d* represents the dimensionality of the problem. In this situation, the mathematical formula can be given as follows:

$$BS^k=\frac{\sum_{i=1}^{p}X_i^k}{p}, \begin{cases} i=1,2,\ldots,p. \\ k=1,2,\ldots,n. \end{cases} \quad (11)$$

$$BE^k=\frac{\sum_{i=1}^{p}E_i^k}{p}, \begin{cases} i=1,2,\ldots,p. \\ k=1,2,\ldots,n. \end{cases} \quad (12)$$

Where as E_i^k and X_i^k indicate the k^{th} layer's main function value and location of i^{th} candidate solution, BE^k and BS^k signify the binding energy and state of k^{th} layers; *m* signifies the overall amount of solution candidates, and the binding state and energy of the atoms are evaluated by the following equation:

$$BS=\frac{\sum_{i=1}^{m}X_i}{m}, i=1,2,\ldots,m. \quad (13)$$

$$BE=\frac{\sum_{i=1}^{m}E_i}{m}, i=1,2,\ldots,m. \quad (14)$$

Whereas E_i and X_i are the i^{th} solution candidate's objective function value and location in the atom; BE and BS show the binding energy and states of the atom. In this approach, the subsequent formulation can be employed to update the position of the solution candidate:

$$X_{i+1}^k=X_i^k+\frac{\alpha_i\times\left(\beta_i\times LE-\gamma_i\times BS\right)}{k}, \begin{cases} i=1,2,\ldots,p. \\ k=1,2,\ldots,n. \end{cases} \quad (15)$$

In Eq. (15), BS refers to the binding state of atoms; α_i, β_i, and γ_i show the vectors, involving arbitrary numbers within (0,1) and evaluate the quantity of released energy; the past and present locations for the i^{th} solution candidate of k^{th} layers are X_i^k and X_{i+1}^k, correspondingly; LE shows the solution candidate with the low atomic energy level.

Once the energy level of the proposed solution in the presented layer is less than the layer's binding energy $\left(E_i^k<BE^k\right)$, photon absorption can be assessed. In the

presented method, the subsequent formula defines the position updating of the solution candidate:

$$X_{i+1}^{k} = X_{i}^{k} + \alpha_i \times \left(\beta_i \times LE^{k} - \gamma_i \times BS^{k}\right), \begin{cases} i = 1,2,\ldots,p. \\ k = 1,2,\ldots,n. \end{cases} \quad (16)$$

In Eq. (16), LE^k indicates the solution candidate of the k^{th} layer with the low energy level; the past and present locations for the i^{th} solution candidate of ^{kth} layers are X_i^k and $X_{i+1}^k; BS^k$ denotes the binding state of k^{th} layers; α_i, β_i *and* γ_i shows the vector, or computes the amount of energy absorbed, involving uniformly distributed random integer within [0,1].

Assume the random number (ø) for all the electrons is lower than PR (<PR). The transit of electrons across dissimilar layers around the nucleus is based on other processes, namely, particle magnetic fields or interactions, which leads to energy emission or absorption because the photons' impact on electrons is implausible. The method whereby the positions of solution candidates are updated in consideration of this impact is given below:

$$X_{i+1}^{k} = X_{i}^{k} + r_i, \begin{cases} i = 1,2,\ldots,p. \\ k = 1,2,\ldots,n. \end{cases} \quad (17)$$

In Eq. (17), r_i shows the vector, involving randomly produced numbers within [0, 1]; the past and present positions for the ith solution candidate for the k^{th} layers are X_i^k and X_{i+1}^k

During this case, the AOSA can be utilized for determining the hyperparameter concerned in the DLSTM approach. The MSE is assumed as the main function and is determined as:

$$MSE = \frac{1}{T}\sum_{j=1}^{L}\sum_{i=1}^{M}\left(y_j^i - d_j^i\right)^2 \quad (18)$$

In which, M and L stand for the outcome value of the layer and data correspondingly, y_j^i and d_j^i denote the accomplished and suitable magnitudes for j^{th} unit in the outcome layer of networks from the time t.

4. Results and discussion

In this section, the performance of the AOSADL-APM technique is studied under different aspects. Table 1 signifies the prediction outcome of the AOSADL-APM algorithm with varying variables. The outcome highlighted that the AOSADL-APM technique predicts the pollutants properly with minimal MSE and MAE values.

The classification outcome of the AOSADL-APM technique can test utilizing a database comprising 22321 instances and two class labels as defined in Table 2.

Figure 3 demonstrates the confusion matrices created by the AOSADL-APM method under 80:20 and 70:30 of the TR phase/TS phase. The outcomes implied the effectual recognition of the pollutant and non-pollutant samples under all classes.

The pollutant classification results of the AOSADL-APM technique with 80:20 of the TR phase/TS phase are portrayed in Table 3 and Figure 4. The results infer that the AOSADL-APM technique properly recognizes the non-pollutant and pollutant samples. With an 80% TR phase, the AOSADL-APM technique offers an average $accu_y$ of 97.30%, $prec_n$ of 96.93%, $reca_1$ of 97.30%, F_{score} of 97.11%, and AUC_{score} of 97.30%. Besides, with a 20% TS phase, the AOSADL-APM algorithm gains an average $accu_y$ of 97.78%, $prec_n$ of 97.63%, $reca_1$ of 97.78%, F_{score} of 97.70%, and AUC_{score} of 97.78%.

Table 1. Prediction outcome of the AOSADL-APM algorithm under varying variables

Variables	Training Set	Testing Set	Validation Set
		MSE	
CO	0.037	0.034	0.030
Ozone	0.498	0.448	0.053
SO2	0.297	0.396	0.426
NO2	0.037	0.029	0.056
PM2.5	0.286	0.157	0.241
		MAE	
CO	0.075	0.088	0.094
Ozone	0.089	0.087	0.104
SO2	0.106	0.110	0.108
NO2	0.097	0.076	0.113
PM2.5	0.111	0.108	0.110

Table 2. Details on database

Class	No. of Instances
Non-Pollutant	15738
Pollutant	6583
Total Number of Instances	**22321**

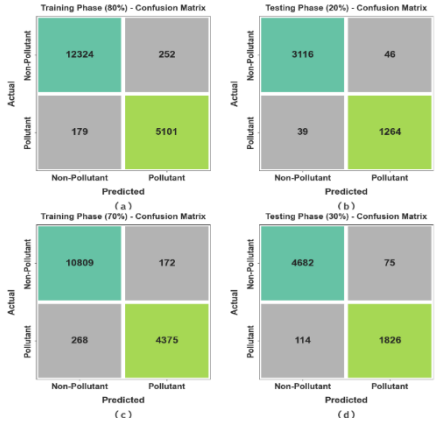

Figure 3. Confusion matrices of (a-b) 80:20 of TR phase/TS phase and (c-d) 70:30 of TR phase/TS phase

Table 3. Pollutant classifier outcome of AOSADL-APM approach at 80:20 of TR phase/TS phase

Classes	$Accu_y$	$Prec_n$	$Reca_1$	F_{score}	AUC_{score}
		TR phase (80%)			
Non-Pollutant	98.00	98.57	98.00	98.28	97.30
Pollutant	96.61	95.29	96.61	95.95	97.30
Average	**97.30**	**96.93**	**97.30**	**97.11**	**97.30**
		TS phase (20%)			
Non-Pollutant	98.55	98.76	98.55	98.65	97.78
Pollutant	97.01	96.49	97.01	96.75	97.78
Average	97.78	97.63	97.78	97.70	97.78

The pollutant classification outcome of the AOSADL-APM algorithm at 70:30 of the TR phase/TS phase is represented in Table 4 and Figure 5. The outcome stated that the AOSADL-APM algorithm properly recognizes the non-pollutant and pollutant samples. With 70% TR phase, the AOSADL-APM system attain an average acc_y of 96.33%, $prec_n$ of 96.90%, $reca_1$ of 96.33%, F_{score} of 96.61%, and AUC_{score} of 96.33%. Besides, with a 30% TS phase, the AOSADL-APM algorithm achieves an average acc_y of 96.27%, $prec_n$ of 96.84%, $reca_1$ of 96.27%, F_{score} of 96.55%, and AUC_{score} of 96.27%.

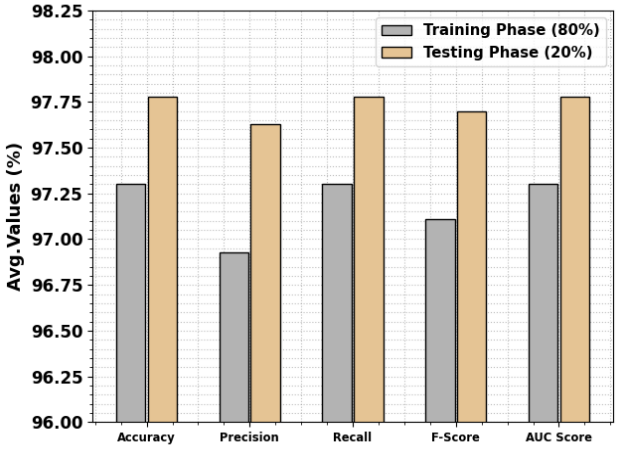

Figure 4. Average of AOSADL-APM algorithm with 80:20 of TR phase/TS phase

Table 4. Pollutant classifier outcome of AOSADL-APM system at 70:30 of TR phase/TS phase

Class	$Accu_y$	$prec_n$	$Reca_1$	F_{score}	ACC_s
		TR phase (70%)			
Non-Pollutant	98.43	97.58	98.43	98.01	96.33
Pollutant	94.23	96.22	94.23	95.21	96.33
Average	**96.33**	**96.90**	**96.33**	**96.61**	**96.33**
		TS phase (30%)			
Non-Pollutant	98.42	97.62	98.42	98.02	96.27
Pollutant	94.12	96.05	94.12	95.08	96.27
Average	**96.27**	**96.84**	**96.27**	**96.55**	**96.27**

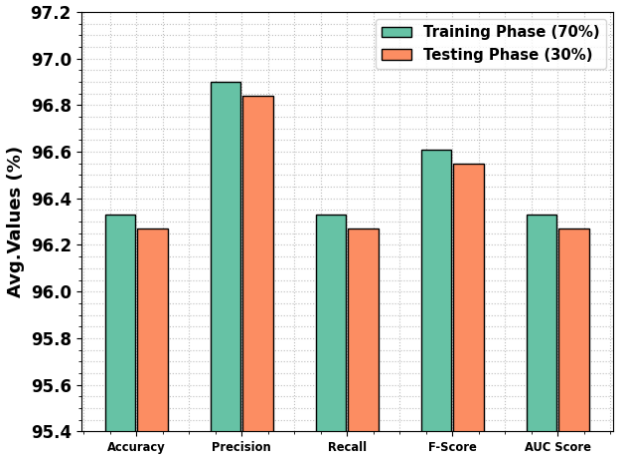

Figure 5. Average of AOSADL-APM method at 70:30 of TR phase/TS phase

To estimate the performance of the AOSADL-APM system at 80:20 of the TR phase/TS phase, TR and TS $accu_y$ curves are determined, as revealed in Figure 6. The TR and TS $accu_y$ curves establish the performance of the AOSADL-APM method over several epochs. The figure offers meaningful details regarding the learning task and generalization capabilities of the AOSADL-APM approach. With an increase in epoch count, it is perceived that the TR and TS $accu_y$ curves get improved. It is observed that the AOSADL-APM approach obtains enhanced testing accuracy which can recognize the patterns in the TR and TS data.

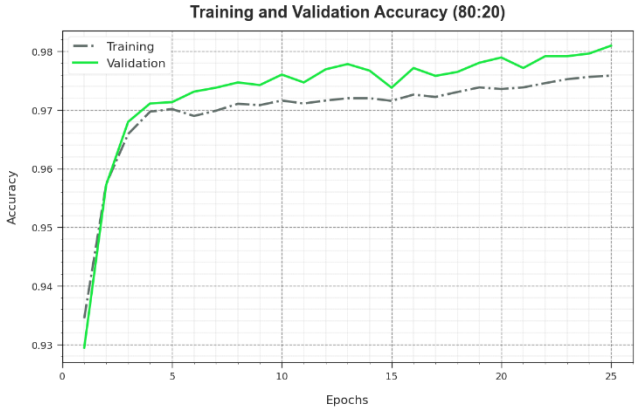

Figure 6. $Accu_y$ curve of AOSADL-APM algorithm with 80:20 of TR phase/TS phase

Figure 7 exhibits the overall TR and TS loss values of the AOSADL-APM algorithm at 80:20 of the TR phase/TS phase epochs. The TR loss displays the method loss gets lesser over epochs. Primarily, the loss values get reduced as the model modifies the weight to diminish the predictive error on the TR and TS data. The loss curves demonstrate the extent to which the model fits the training data. It is experimental that the TR and TS loss is steadily decreased and portrayed that the AOSADL-APM approach effectually learns the patterns exhibited in the TR and TS data. It is also observed that the AOSADL-APM system adjusts the parameters to minimize the discrepancy between the prediction and the original training label.

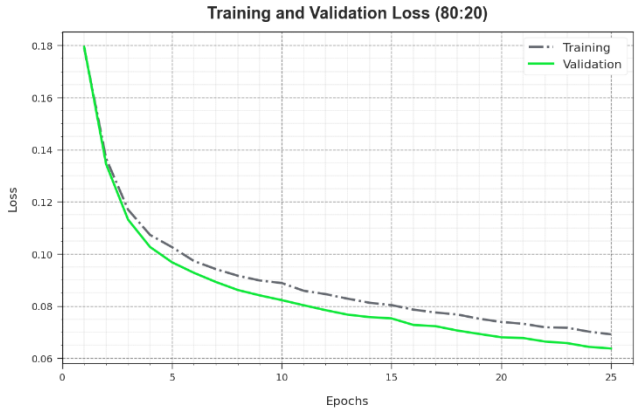

Figure 7. Loss curve of AOSADL-APM algorithm with 80:20 of TR phase/TS phase

The PR curve of the AOSADL-APM approach at 80:20 of the TR phase/TS phase is established by plotting the precision against recall as defined in Figure 8. The results confirm that the AOSADL-APM system gains better PR values under all classes. The figure depicts that the model learns to

recognize various class labels. The AOSADL-APM system accomplishes higher outcomes in the recognition of positive samples with minimal false positives.

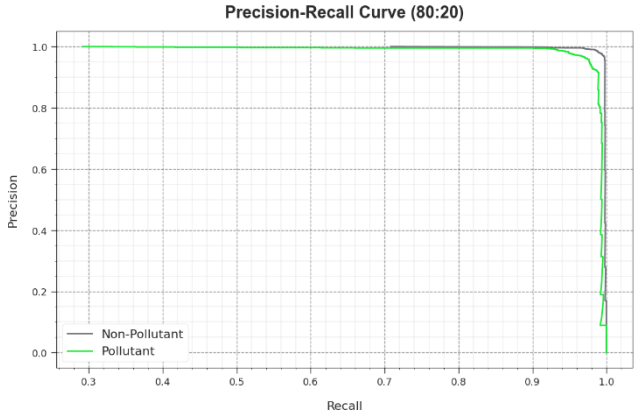

Figure 8. PR curve of AOSADL-APM algorithm with 80:20 of TR phase/TS phase

The ROC curves provided by the AOSADL-APM algorithm at 80:20 of the TR phase/TS phase are exemplified in Figure. 9, which has the ability discriminate the classes. The figure indicates valuable insights into the trade-off between the TPR and FPR rates over distinct classification thresholds and varying numbers of epochs. It presents the accurate predictive outcome of the AOSADL-APM algorithm on the classification of various classes.

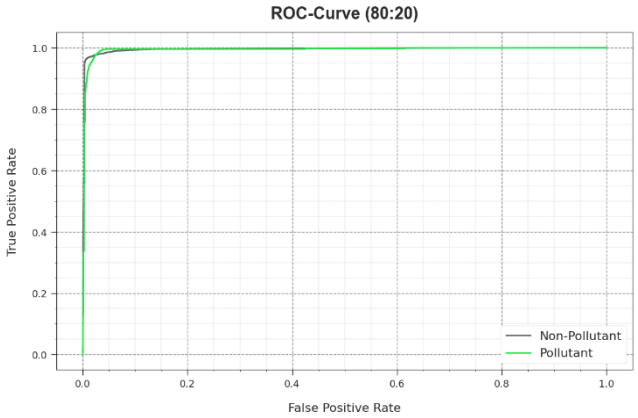

Figure 9. ROC curve of AOSADL-APM system at 80:20 of TR phase/TS phase

Table 5. Comparative outcomes of AOSADL-APM system with recent methodologies

Methods	$Prec_n$	$Reca_1$	$Accu_y$	F_{score}
PCA SVR-RBF	60.70	60.80	95.20	60.70
SVR-RBF	61.80	62.00	96.00	61.90
Decision tree	90.80	69.40	87.40	58.60
SVM Model	92.40	72.50	91.70	74.50
ANN Model	94.50	76.30	94.50	78.80
OAI-AQPC	97.20	96.40	96.20	97.30
AOSADL-APM	97.63	97.78	97.78	97.70

Table 5 reports a comparison study of the AOSADL-APM methodology with recent models from Tamilvizhi T., *et al.* (2022)., Hamza, M.A., *et al.* (2022) and Surendran R. *et al.* (2023). Figure 10 inspects the results of the AOSADL-APM algorithm with existing methodologies in terms of $accu_y$. The outcome highlights the higher solution of the AOSADL-APM technique. Based on $accu_y$, the AOSADL-APM technique offers increasing $accu_y$ of 97.78% while the PCA SVR-RBF, SVR-RBF, DT, SVM, ANN, and OAI-AQPC models obtain decreasing $accu_y$ of 95.20%, 96%, 87.40%, 91.70%, 94.50%, and 96.20% correspondingly.

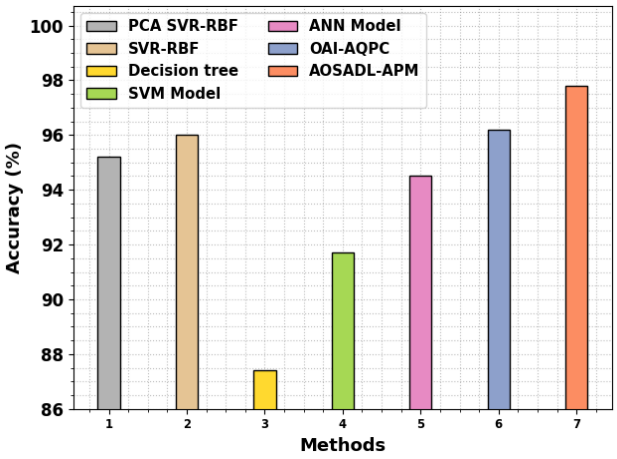

Figure 10. $Accu_y$ outcome of AOSADL-APM algorithm with recent approaches

Figure 11 demonstrates the outcome of the AOSADL-APM system with other methods in terms of $prec_n$, $reca_1$, and F_{score}. The simulation value depicts the better outcome of the AOSADL-APM algorithm. Based on $prec_n$, the AOSADL-APM system attains a higher $prec_n$ of 97.63% while the PCA SVR-RBF, SVR-RBF, DT, SVM, ANN, and OAI-AQPC systems obtain decreasing $prec_n$ of 60.70%, 61.80%, 90.80%, 92.40%, 94.50%, and 97.20% correspondingly. In addition, based on $reca_1$, the AOSADL-APM technique offers an increasing $reca_1$ of 97.78% while the PCA SVR-RBF, SVR-RBF, DT, SVM, ANN, and OAI-AQPC approaches reach a lesser $reca_1$ of 60.80%, 62%, 69.40%, 72.50%, 76.30%, and 96.40% respectively. Eventually, based on F_{score}, the AOSADL-APM technique offers an enhanced F_{score} of 97.70% while the PCA SVR-RBF, SVR-RBF, DT, SVM, ANN, and OAI-AQPC algorithms gain a lesser F_{score} of 60.70%, 61.90%, 58.60%, 74.50%, 78.80%, and 97.30% respectively.

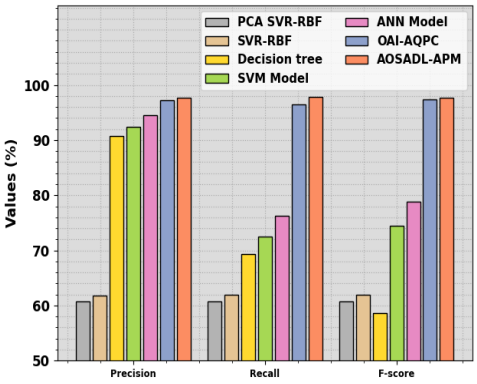

Figure 11. $Prec_n$, $Reca_1$, and F_{score} outcome of AOSADL-APM algorithm with recent approaches

Table 6 and Figure 12 examine the computation time (CT) results of the AOSADL-APM algorithm with recent approaches. The outcome highlights the higher outcome of the AOSADL-APM technique. Based on CT, the AOSADL-APM technique offers lesser CT of 1.35s while the PCA SVR-RBF, SVR-RBF, DT, SVM, ANN, and OAI-AQPC models achieve improved CT of 3.98s, 3.53s, 3.78s, 5.45s, 4.35s, and 2.47s correspondingly.

These performances confirmed the better solution of the AOSADL-APM technique for air pollution monitoring.

Table 6. CT outcome of AOSADL-APM algorithm with recent approaches

Methods	Computational Time (sec)
PCA SVR-RBF	3.98
SVR-RBF	3.53
Decision tree	3.78
SVM Model	5.45
ANN Model	4.35
OAI-AQPC	2.47
AOSADL-APM	1.35

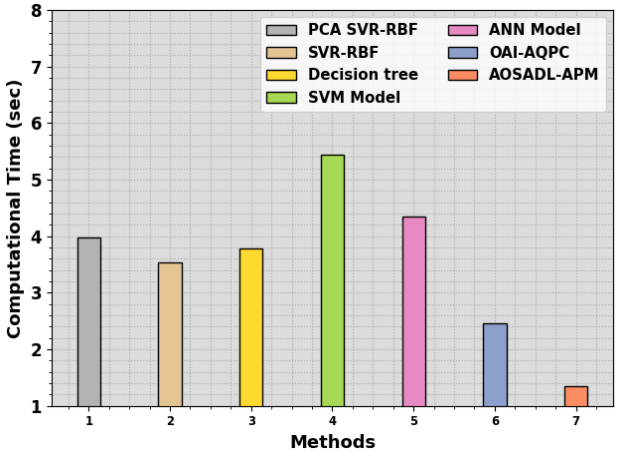

Figure 12. CT outcome of AOSADL-APM algorithm with recent approaches

5. Conclusion

In this study, we have presented an automated air pollution monitoring approach named the AOSADL-APM approach. The purpose of the AOSADL-APM technique is to predict and classify the presence of air pollutants. In the presented AOSADL-APM technique, three subprocesses are involved, namely, data normalization, DLSTM-based prediction, and AOSA-based hyperparameter tuning. In the presented AOSADL-APM technique, the min-max normalization approach is applied for data preprocessing. For air pollution prediction and classification, the AOSADL-APM method applies the DLSTM system. To improve the performance of the AOSADL-APM methodology, the AOSA-based hyperparameter tuning has been developed. The simulation results of the AOSADL-APM technique were tested using the benchmark dataset. The widespread outcomes analyzed the optimum solution of the AOSADL-APM algorithm compared to existing approaches. In the future, the performance of the AOSADL-APM algorithm will improve and utilize hybrid DL models for enhanced detection efficiency at real-time.

Ethics declarations

Funding statement

No funding was received for this study.

Acknowledgment

The authors would like to thank the Rajalakshmi Institute of Technology, SRM Institute of Science and Technology, Panimalar Engineering College, and Amrita Vishwa Vidyapeetham for providing the resources.

Data availability statement

Available Based on Request. The datasets generated and or analyzed during the current study are not publicly available due to the extension of the submitted research work. They are available from the corresponding author upon reasonable request.

Conflict of Interest

The authors declare they have no conflicts of interest to report regarding the present study.

References

Abirami S. and Chitra P. (2023). Probabilistic air quality forecasting using deep learning spatial–temporal neural network. *GeoInformatica,* **27**, 2, 199–235.

Arsov M., Zdravevski E., Lameski P., Corizzo R., Koteli N., Gramatikov S., Mitreski K. and Trajkovik, V. (2021), Multi-horizon air pollution forecasting with deep neural networks. *Sensors,* **21,** 4, 1235.

Dairi A., Harrou F., Khadraoui S. and Sun Y., (2021). Integrated multiple directed attention-based deep learning for improved air pollution forecasting. *IEEE Transactions on Instrumentation and Measurement*, **70**, 1–15.

Drewil G.I. and Al-Bahadili R.J. (2022). Air pollution prediction using LSTM deep learning and metaheuristics algorithms. *Measurement: Sensors*, **24,** 100546.

Du S., Li T., Yang Y. and Horng S.J., (2019), Deep air quality forecasting using hybrid deep learning framework. *IEEE Transactions on Knowledge and Data Engineering*, **33**, 6, 2412–2424.

Elshaboury N., Mohammed Abdelkader E. and Al-Sakkaf A. (2023), Convolutional neural network-based deep learning model for air quality prediction in October city of Egypt. *Construction Innovation.*

Gilik A., Ogrenci A.S. and Ozmen A. (2022), Air quality prediction using CNN+ LSTM-based hybrid deep learning architecture. Environmental science and pollution research, 1–19.

Gu Y., Li B. and Meng Q. (2022). Hybrid interpretable predictive machine learning model for air pollution prediction. *Neurocomputing,* **468,** 123–136.

Hamza, M.A., Shaiba, H., Marzouk, R., Alhindi, A., Asiri, M.M., Yaseen, I., Motwakel, A. and Rizwanullah, M. (2022), Big Data Analytics with Artificial Intelligence Enabled Environmental Air Pollution Monitoring Framework. *Computers, Materials & Continua*, **73,** 2.

Hardini M., Sunarjo R.A., Asfi M., Chakim M.H.R. and Sanjaya Y.P.A. (2023), Predicting Air Quality Index using Ensemble Machine Learning. ADI Journal on Recent Innovation, **5**(1Sp), 78–86.

Heydari A., Majidi Nezhad M., Astiaso Garcia D., Keynia F. and De Santoli L. (2022). Air pollution forecasting application based

on deep learning model and optimization algorithm. *Clean Technologies and Environmental Policy,* 1–15.

Huang L., Liu S., Yang Z., Xing J., Zhang J., Bian J., Li S., Sahu S.K., Wang S. and Liu T.Y. (2021), Exploring deep learning for air pollutant emission estimation. *Geoscientific Model Development,* **14**, 7, 4641–4654.

Jamei M., Ali M., Malik A., Karbasi M., Sharma E. and Yaseen Z.M. (2022), Air quality monitoring based on chemical and meteorological drivers: Application of a novel data filtering-based hybridized deep learning model. *Journal of Cleaner Production*, **374**, p.134011.

Lin C.Y., Chang Y.S. and Abimannan S. (2021). Ensemble multifeatured deep learning models for air quality forecasting. *Atmospheric Pollution Research*, **12**, 5, 101045.

Santhanaraj R. K., Rajendran S., Romero C. A. T., and Murugaraj, S. S. (2023), Internet of Things Enabled Energy Aware Metaheuristic Clustering for Real Time Disaster Management. *Comput. Syst. Sci. Eng.,* **45**, 1561–1576.

Shu Y., Ding C., Tao L., Hu C. and Tie Z. (2023), Air Pollution Prediction Based on Discrete Wavelets and Deep Learning. *Sustainability*, **15**, 9, 7367.

Sonawani S., Patil K. and Chumchu P. (2021), NO2 pollutant concentration forecasting for air quality monitoring by using an optimised deep learning bidirectional GRU model. International Journal of Computational Science and Engineering, **24,** 1, 64–73.

Surendran R., Alotaibi Y. and Subahi A.F. (2023), Wind Speed Prediction Using Chicken Swarm Optimization with Deep Learning Model. *Computer Systems Science & Engineering*, **46,** 3.

Surendran R., Alotaibi Y. and Subahi, A.F. (2023), Lens-Oppositional Wild Geese Optimization Based Clustering Scheme for Wireless Sensor Networks Assists Real Time Disaster Management. *Comput. Syst. Sci. Eng*., **46,** 835–851.

Surendran R., Tamilvizhi T., and Lakshmi, S. (2021), Integrating the Meteorological Data into a Smart City Service Using Cloud of Things (CoT). In Emerging Technologies in Computing: 4th EAI/IAER International Conference, iCETiC 2021, Virtual Event, August 18–19, 2021, *Springer International Publishing,* **4,** 94–111

Tamilvizhi T., Surendran R., Romero C.A.T. and Sadish M. (2022), Privacy preserving reliable data transmission in cluster based vehicular adhoc networks*, Intelligent Automation & Soft Computing*, **34**, 1265–1279.

Tang W., Yang S. and Khishe M. (2023). Profit prediction optimization using financial accounting information system by optimized DLSTM. *Heliyon.*

Wang S., Ren Y., Xia B., Liu K. and Li H. (2023), Prediction of atmospheric pollutants in urban environment based on coupled deep learning model and sensitivity analysis. *Chemosphere*, **331**, 138830.

Wardana I.N.K., Gardner J.W. and Fahmy S.A. (2021), Optimising deep learning at the edge for accurate hourly air quality prediction. *Sensors*, **21**, 4, 1064.

Wu C.L., Song R.F., Zhu X.H., Peng Z.R., Fu Q.Y. and Pan J. (2023). A hybrid deep learning model for regional O3 and NO2 concentrations prediction based on spatiotemporal dependencies in air quality monitoring network. *Environmental Pollution*, **320,** 121075.